Journal of Achievements in Materials and Manufacturing Engineering
International Scientific Journal published monthly by the World Academy of Materials and Manufacturing Engineering

Comparison of impact delaminations in CFRP using different test methods

I. Ehrlich [a], H. Dinnebier [b,*], C. Jost [a]

[a] Regensburg University of Applied Sciences, Faculty of Mechanical Engineering, Laboratory of Composite Technology (LFT), Galgenbergstrasse 30, 93053 Regensburg, Germany
[b] Bundeswehr Research Institute for Materials and supplies, Institutsweg 1, 85435 Erding, Germany,
Corresponding e-mail address: heinrichdinnebier@bundeswehr.org

ABSTRACT

Purpose: of this paper is comparison of impact delaminations in CFRP using different test methods.

Design/methodology/approach: A comparison is made between the results of well-established techniques such as Ultrasonic Testing or micrographic cross-sections with the results of Microfocus Computed X-Ray Tomography.

Findings: The findings show that both Ultrasonic Testing and µCT show a linear correlation between impact energy and delaminated area. However, µCT is able to detect significantly larger delaminated areas. Other findings were that the undamaged zone immediately underneath the contact point of the impactor is not a cylinder but a cone segment. The higher density of that compacted area could also be visualized.

Research limitations/implications: The correlation between main impact parameters could be shown on the base of state of the art non-destructive testing.

Originality/value: Impact delaminations in carbon fiber reinforced plastic have generated in a well-defined manner and a comparison is made between the results of well-established techniques such as Ultrasonic Testing (UT) or micrographic cross-sections with the results of Microfocus Computed X-Ray tomography (µCT).

Keywords: Impact; Delamination; Ultrasonic testing; Microfocus computed X-Ray tomography; Micrograph

Reference to this paper should be given in the following way:

I. Ehrlich, H. Dinnebier, C. Jost, Comparison of impact delaminations in CFRP using different test methods, Journal of Achievements in Materials and Manufacturing Engineering 73/2 (2015) 128-138.

METHODOLOGY OF RESEARCH

1. Introduction

Carbon fiber reinforced plastics (CFRP) have established themselves in a wide field of applications. As its use grows from the tightly regulated aerospace field to the "wild" consumer area, e. g. in automotive use, the probability of damage increases. Since CFRP can exhibit such undesired problems as barely visible impact damage (BVID), there is an urgent need for a correct measurement of the actual damage size.

The characterization of impact delaminations by Ultrasonic Testing (UT) has been a well-established technique for decades. However, this method has some limitations. Most importantly, UT is essentially blind after the first delaminated layer. Therefore, correct measurements of multilayer delaminations are hard to obtain with this method. Microfocus Computed X-Ray Tomography does not have this limitation since it is a technique that can penetrate and analyze the whole volume. On the other hand, there can be limits to the detectability of very thin delaminations with so called kissing surfaces.

2. Material and method

2.1. Material

For all specimens the unidirectional (UD) epoxy system Hexcel 8552/IM7 [1] was used. 32 prepreg layers were stacked quasi-isotropically with a symmetry layer in the middle: $[[+45/0/-45/90]_4]_s$ according to DIN EN 7000-11 [2]. Sample thickness of all specimen was about 4 mm. Manufacturing and curing were performed according to the manufacturers guidelines with curing at 185°C. Fiber-volume content and porosity were measured according to DIN EN 2564 [3]. The resulting fiber-volume content was 60 % with no detectable porosity. Cure quality was checked using differential scanning calorimetry (DSC). For all specimens the remaining enthalpy was found to be less than 0.3 J/g. The specimens were finally cut with a water-cooled diamond saw into length of 150 mm x 100 mm. Homogeneity of the laminate was checked by ultrasonic testing.

2.2. Impact testing

The impact testing was performed according to the AIRBUS Industry Test Method AITM 1.0010 [4]. Impact testing was done on an Instron Fractoris impact machine for most of the specimens. For comparison some of the impacts were made using an Instron CEAST 9350 machine. All specimens were impacted with an instrumented 20 mm spherical steel impactor. Impact energy was varied by attaching additional mass segments to the impactor. The energy levels were: 3.14 J; 6.13 J; 7.12 J; 8.65 J; 9.28 J and 12.14 J.

Drop height was kept at 170 mm for all specimens except for the energy levels 3.14 J (85 mm) and 9.28 J (306 mm, CEAST 9350).

The impact velocity v can be approximately calculated from the drop height. The resulting velocities were $1.29\ \mathrm{m/s}$ $1.83\ \mathrm{m/s}$ and $2.45\ \mathrm{m/s}$ for drop heights of 85 mm, 170 mm and 306 mm. Following the definitions of CANTWELL and MORTON [5] these impact velocities of less than $10\ \mathrm{m/s}$ can be considered as so called low velocity impacts.

2.3. Ultrasonic testing

For ultrasonic testing a Hillger HFUS 2000 scanning system [6] was used in an impulse/echo setup. A mechanical step size of 0.1 mm and a 20 MHz broadband ultrasonic probe were selected to ensure adequate spatial resolution. The ultrasonic probe had a spectral bandwidth of 17.6 MHz when looking at a 6 dB drop from the peak of the transfer function. The specimens were immersed in water for optimum coupling conditions. The whole scan data was stored in a 3D file to enable various methods of analysis. Analysis was performed with the software Oculus V1.30. To determine the total defect size, the defect echo was used as well as the total attenuation with a glass plate as auxiliary reflector. This way the sound had to pass through the full thickness of the specimen twice, enhancing total attenuation. The evaluation of the total defect size was done by analyzing the images from ultrasonic testing with an own written program for Matlab version 2011 R.

2.4. Micrographic cross-section

As a further method of comparison, micrographic cross-sections were made on some specimens. Sections measuring 35 mm x 10 mm x 4 mm were cut out at the impact area. Cutting was done with a water-cooled diamond saw to minimize additional damage. The specimens were then embedded into an epoxy matrix and polished in three steps up to a grain size of 4000. Afterwards they were fine polished in a 3 µm and 1 µm diamond suspension. Microscopic inspection was performed with an Olympus AX70 digital microscope and the software Analysis Pro 5.0.

2.5. Microfocus computed X-Ray tomography

µCT was performed on a V-TOME XL 300 system using both a 300 kV microfocus and a 180 kV nanofocus x-ray source. In most scans, 1440 projections of 2024 x 2024 pixel resolution were combined into a digital volume of the specimen. All specimens were scanned twice. The first scan included the whole specimen and was used to determine the actual dimensions of the delaminations. In the second, high-resolution scan, a region of interest was selected in order to get the best possible resolution and still include the full

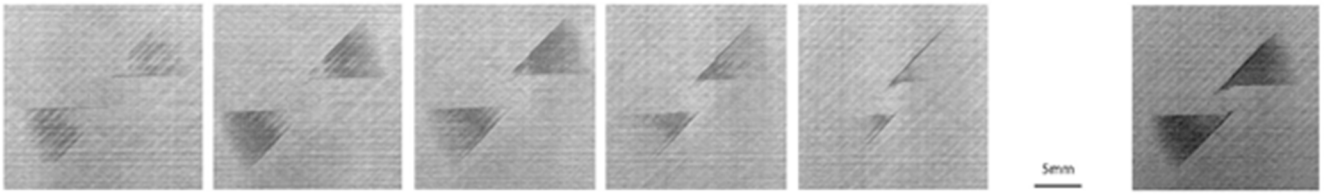

Fig. 1. Combination of several µCT cross cut layers (left) into one single thick slab projection (right)

delaminated area into the digital volume. In the high-resolution scans, voxel sizes between 16 µm and 28 µm have been obtained, depending on the size of the delaminated area. For analysis, only the high-resolution scans have been used. Data analysis and visualization was done with VG Studio Max 2.2 and Analysis 5.0. Since the scan resolution of the high resolution scans was considerably finer than the thickness of a CFRP lamina, each delamination was visible in several µCT layers with a considerable overlap between the images. In order to eliminate this overlap, it was necessary to project those layers in one single image.

This was possible using the "thick slab" tool in VG Studio – Figure 1. By defining a thick slab thickness of 100µm and displaying only the pixels within those layers with the minimum brightness, a clear projection of all parts of the delamination was obtained. The delamination area in that projection was then also analyzed with the software Analysis 5.0.

3. Results

3.1. Impact testing

Different impact parameters were used to show the main correlations. These correlations can be used in the future to predict impact damages. During impact tests parameters like contact force, impact indentation and time were recorded. Figure 2 shows the impact force versus time in light blue. The contact force increases after the impactor has reached the surface of the specimen.

The impact energy is stored as elastic energy in the specimen until the moment when the force reaches the point of crack initiation.

In Figure 2 the quasi-linear force/time relation ends at $t = 0.51$ ms and force drops from $F = 7{,}865$ N to $F = 2{,}921$ N. The abrupt reduction of bending stiffness due to the brittle impact damage behavior of the carbon fiber reinforced plastics is the reason for the drop in impact force [7, 8].

After the first drop the contact force increases again. Smaller force drops mark the crack growth in the specimen. In this test the impact force reaches its maximum after app. 2 ms.

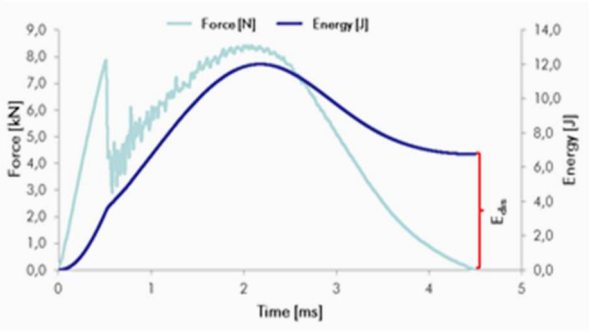

Fig. 2. Force vs. time and energie vs. time diagram. Constant impact hight of h=170 mm, impact velocity of v=1.83 m/s and impact mass of m_imp=7.25 kg

The stored elastic energy in the specimen accelerates the impactor in the opposite direction and the contact force is reduced to zero.

The dark blue line shows the impact energy and the dissipated energy E_{dis}. The energy-time curve is the integral of the force-displacement curve.

At the beginning of the experiment the potential energy of the impactor is converted into kinetic energy until contact with the surface of the specimen.

After this point the impactor is decelerated and the impact energy is stored in elastic energy of the plate deflection.

A small amount of energy is dissipated to friction, etc.. At the moment of first failure energy is dissipated due to crack initiation and crack growth. The dissipational part of the total impact energy consists not only of damage growth. Plastic deformations and vibration of the specimen also dissipate energy. For example TAN and SUN [9] as well as CHOI and LIM [10] consider the influence of Hertz' pressure on the dissipation of energy. The dissipated energy can be identified as E_{dis} as the integral of the force-displacement curve over the hole impact time.

Figure 3 illustrates the dissipated energy E_{dis} versus the impact energy E_{imp}. The dissipated part of the energy increases with impact energy. An approximately linear relation is shown in this diagram. This correlation can be interpreted as a direct relation between impact load and impact damage provided that the impact force is higher than the minimum force for damage initiation.

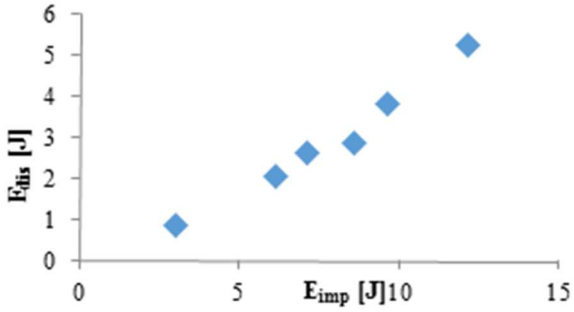

Fig. 3. Dissipative energie E_{dis} versus impact energie E_{imp}.

3.2. Ultrasonic testing

Since the US-software allowed the storage of the full scan data, it was possible to create virtual B-, C- and D-Scans at any location later on.

For analysis, the B-scans were always located in the middle of the impact.

The first layers of the delamination structure can be seen in the C-Scans - Figure 4. Underneath a delamination, US testing is almost blind since most sound energy is reflected there.

In deeper layers of the laminate only those parts of the delaminations are visible which are not blocked by other delaminations above. Therefore, the total size of multiple delaminations is hard to measure. For the upper, unshadowed layers, shape and size of single delaminations can be correctly seen in the C-Scan images. The delamination has the typical peanut- or butterfly-shaped structure.

However, in some cases there is also an unexpected ring around the impact that has roughly the same diameter as the peanut-shaped delamination. Such a ring could be caused by incorrect aperture settings, which would lead to the inclusion of parts of the next delamination one layer further down. However, in this case the aperture was set as narrow as possible specifically to exclude this effect. One possible explanation are diffraction effects at the edge of the lower delamination.

An easy way to measure the total projected damage area of flat specimens is by using the auxiliary reflector technique described in chapter 2.3.

The result is a projection of the total delaminated area. This projection can be easily measured using Oculus or any other image analysis software. It has long been a standard technique to plot this projected area versus the impact energy. This plot is given in Figure 10.

3.3. Micrographic cross-section

Fig 5 shows an overview as well detailed images of a micrographic cross-section. The top picture illustrates the complex damage morphology. Details of this cross-section are given in the bottom pictures. The left bottom picture shows multiple z-shaped cracks as a combination of different types of failure. Several flat cracks (1), i.e. delaminations between two different orientated plies can be seen in the bottom left detail image

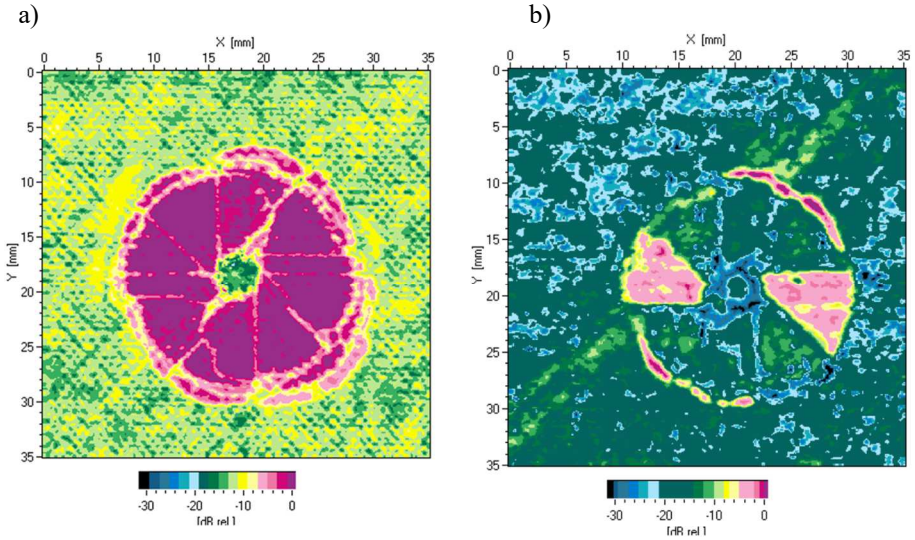

Fig. 4. a) Ultrasonic C-scan (auxiliary reflector) of the impact area after an impact of $E_{imp} = 9.28$ J, b) Typical peanut structure (red triangles) of a wing-like delamination between two single layers with diffent stacking orientation and a ring structure. Measuring depth is 1.45 mm

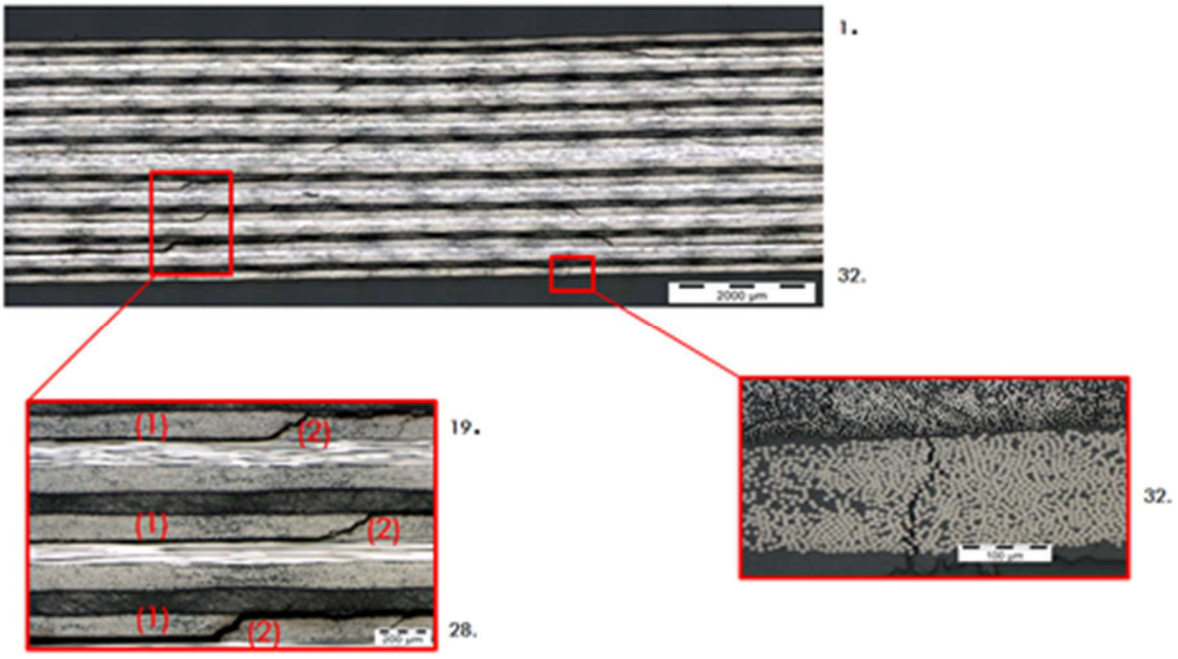

Fig. 5. Detailed view of a micrographic cross-section

The two detail images also show intralaminar cracks (2) between parallel fibers inside a single layer. In cross section images, some plies look very dark due to their low reflectiveness in that orientation. Since cracks also appear as dark lines, it can be hard to find intralaminar cracks within such plies or interlaminar cracks between those and other plies.

The top image of

Fig. 5 also gives a first impression of the cone segment shaped morphology of the impact cracks in a quasi-isotropic laminate. The tip of this cone is located outside the laminate, above the impact side. The bottom side of the cone can be located below the 32nd layer of the laminate which is opposite of the impact area

3.4. Microfocus Computed X-Ray Tomography

Tomography was able to analyze all cracks and delaminations anywhere in the scan volume without any restrictions due to shadowing. This meant that an analysis of the each delaminated area was possible even for overlapping delaminations. As a result, the total sum of the individually measured delaminations was expected to be larger than just the projection of those delaminations, because the projection does not count the overlapping parts. It was also possible to show the crack morphology in more detailed way than had been previously described. In the top view, not only the full extent of the delaminations could be shown. It was even possible to visualize the intralaminar cracks extending from the impact zone – see chapter 3.6.

3.5. Comparison

By comparing results from identical areas of the specimen, the individual advantages and disadvantages of each technique can be demonstrated.

UT gives a very strong and clear indication of the first delamination. Even “kissing”, i.e. weak delaminations can be detected with UT.

Deeper into the material the indications are much less clear and only those parts of a delamination can be seen that are not shadowed from above. The total area of overlapping delaminations is very hard to measure with UT – Figure 6 and 7. Cracks can be found as long as the crack surface is not in parallel to the angle of incidence of the sound waves. In comparison to the other techniques, UT has the lowest resolution due to its large wavelength. In this study the wavelength was about 0.17 mm.

Micrographs can be analyzed at sub-micron resolution which is unmatched by the other two techniques. Even very small cracks can be detected using optical or electron microscopy. However, especially optical microscopy can have problems finding cracks whenever contrast between crack and lamina is weak. Micrographs offer only a view

along the cutting plane. Depth information is almost nonexistent. For information about other parts of the specimen, additional micrographs are necessary. However, even if there are several micrographs on one specimen, it is not really feasible to get comprehensive information throughout the volume. Cracks and delaminations are visible only if the crack direction is not parallel to the cutting plane. Therefore it is hard to analyze or even find the typical peanut shaped delamination structure. The main drawback of micrographs is that their preparation destroys the specimen whereas UT and µCT are non-destructive techniques.

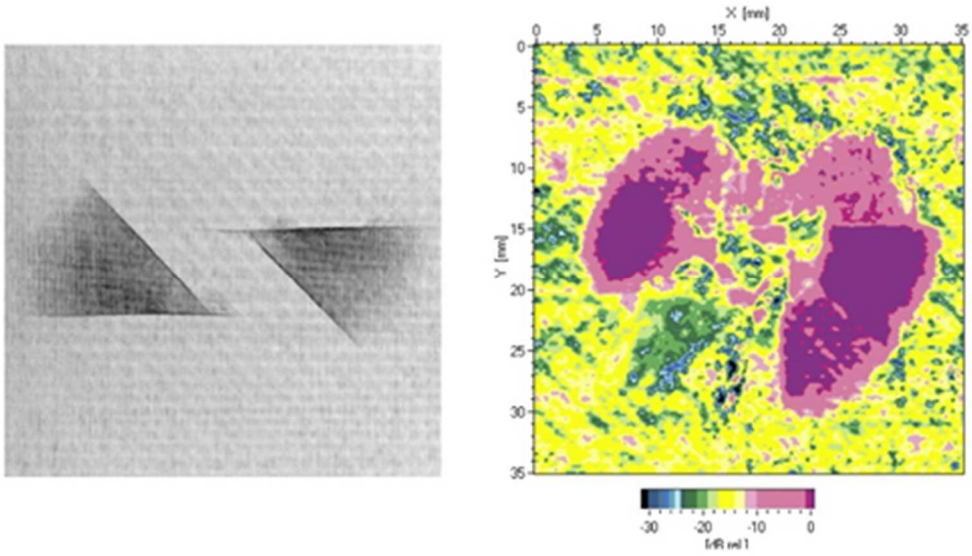

Fig. 6. µCT thick slab picture of one delamination layer and ultrasonic picture of the same layer - .3.25 mm depth

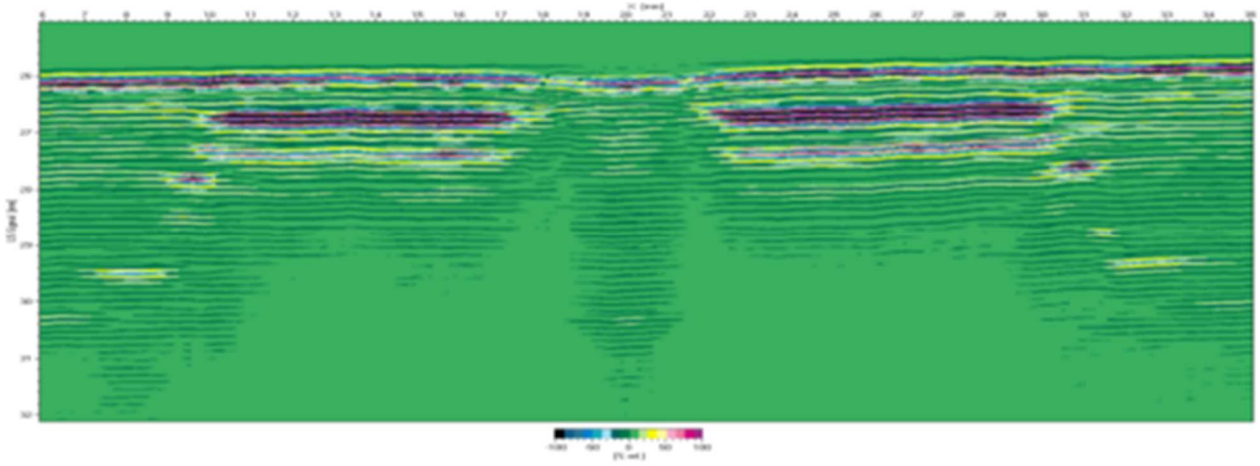

Fig. 7. UT B-Scan – The top delaminations are visible, the lower delamination only show up at the

Even if µCT resolution was lower than in the micrographs, the contrast between cracks /delaminations and material was excellent. Therefore the cone shaped damage morphology was much easier to visualize with µCT than it was in micrographs or UT – see Fig. 8 and Fig. 9.

In thick slab mode µCT can generate a projection of the total delaminated area that is similar to the UT projection.

In addition to the simple projection, the full extent of the cracks and delaminations can be shown.

A layer by layer analysis is possible that can reveal considerably more detail than UT does. µCT offers constant resolution and contrast throughout the whole scanned volume, whereas UT loses contrast with increasing depth. Fig 6 shows how the true shape of one individual

delamination layer is clearly visible using µCT even in deeper layers, while the UT image of the same layer hardly shows the peanut shape anymore.

However, this is true only as long as the delamination causes an opening between the plies that is larger than the µCT resolution. Kissing delaminations can go undetected in µCT whereas they show up in UT.

The total delamination area measured by µCT versus dissipation energy and the delamination projection area measured by UT versus dissipation energy are given in Figure 10.

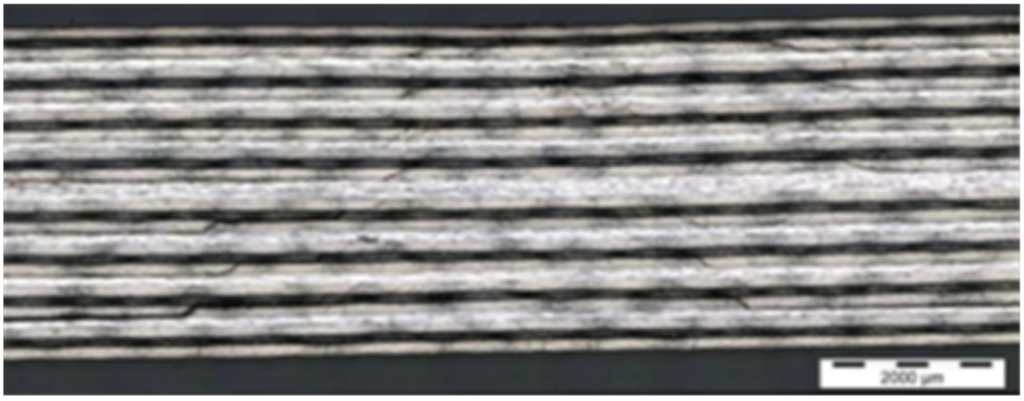

Fig. 8. Micrograph. All delaminations can be seen, although the contrast between the dark layers and cracks along those layers is low

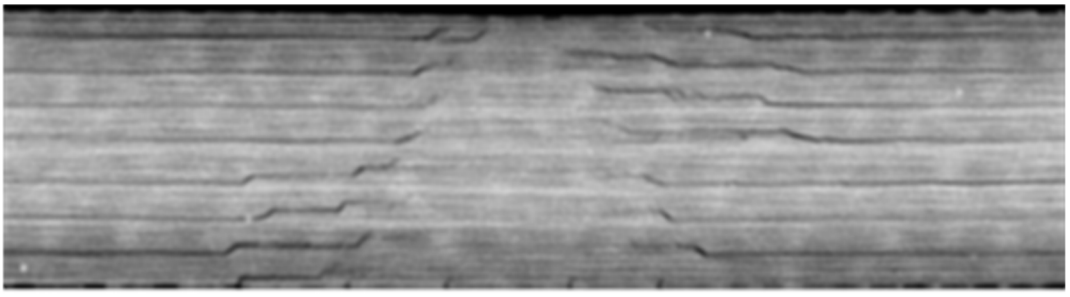

Fig. 9. CT cross-section. resolution is lower than in the micrograph, but the contrast between material and delaminations is high

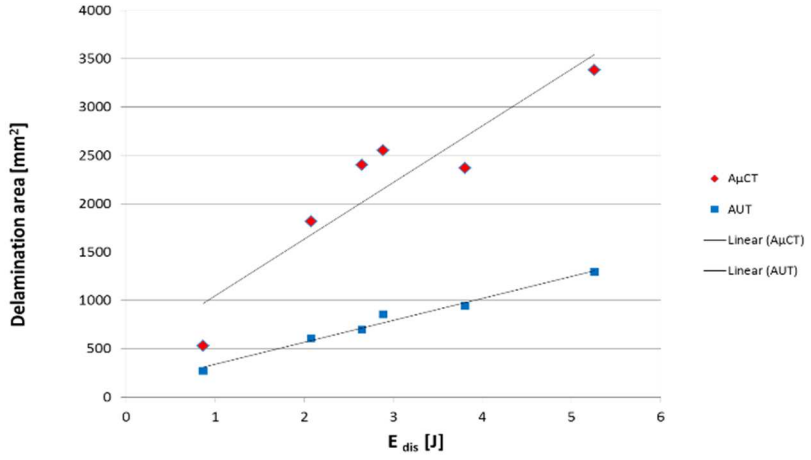

Fig. 10. Damage area vs. dissipated impact energy, red = µCT measurement, blue = UT measurement, quasi-isotropic material

Both measurements of the damage area show a quasi-linear correlation to the dissipated energy during impact. Due to the above discussed effect, the results of µCT measurements are considerably higher than the UT measurements.

The difference between the two measurement types shows a factor of 2.6. This gives an impression of the real damage area as well as the underestimation of the real damage area by UT.

3.6. Additional Findings

Nondestructive testing by µCT provides a new insight into the morphology of impact damage. The delamination structure between two different orientated plies is shown in Figure 11. The point of view is perpendicular to the xy-plane in direction of increasing layer number. Here, the investigated interface is located between the fourth and fifth layer. The layer above is orientated in 90° direction. The layer below is a +45° layer.

The detailed view (1) top right of Figure 11 illustrates the crack in-between the 90° layer as an intralaminar crack. This crack grows within the plie until it reaches the interface to a differently orientated plie. At this point the crack continues its expansion between the differently orientated plies as a plane crack – a so called interlaminar crack or delamination, respectively.

The double and opposite delamination areas between to differently orientated layers again show the shape of a peanut or butterfly. The two delaminations are point symmetric to the center point of the impact contact area.

The radial crack growth with respect to the impact point depends on the impact energy. The delamination growth in angular orientation ends at +45° or -45° respectively.

The angle of delamination area relates to the angle difference in stacking sequence.

The crack continues parallel to the fiber direction of the 45° layer as an intralaminar crack in until it reaches the next interface. Due to the chosen stacking sequence, the rotation of the single delamination areas show in z-direction the structure of a left twisting down going staircase until it reaches the center plane of the laminate. From this point the rotational direction changes in opposite direction. The impact contact area is investigated in Figure 12. The overview picture on the left hand side shows the impact indentation and two significant cracks in the +45° and -45°orientation. The details of the indentation and the cracks can be seen on the top right of Fig. 12. The black spots in the center show the 0.033 mm plastic indentation of the impactor.

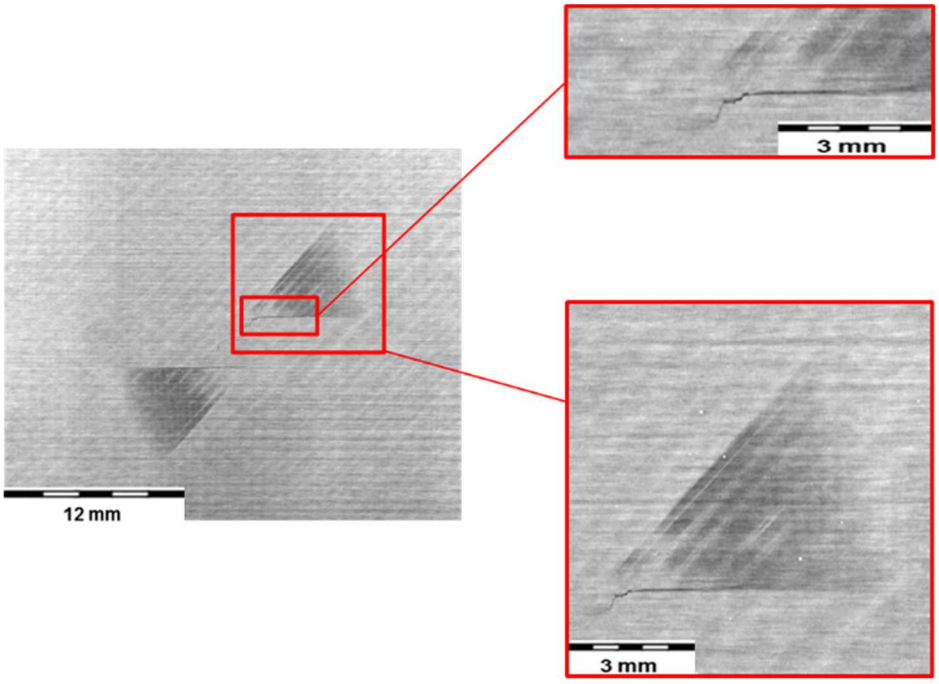

Fig. 11. µCT picture of an impact damage in a depth of 0.4616 mm after an impact of 9.28 J. The detail views show interlaminar, plane cracks between the 90° and +45° layer (interface between layers 4/5) as delamination. The intralaminar crack (1) works as a crack starter/transducer

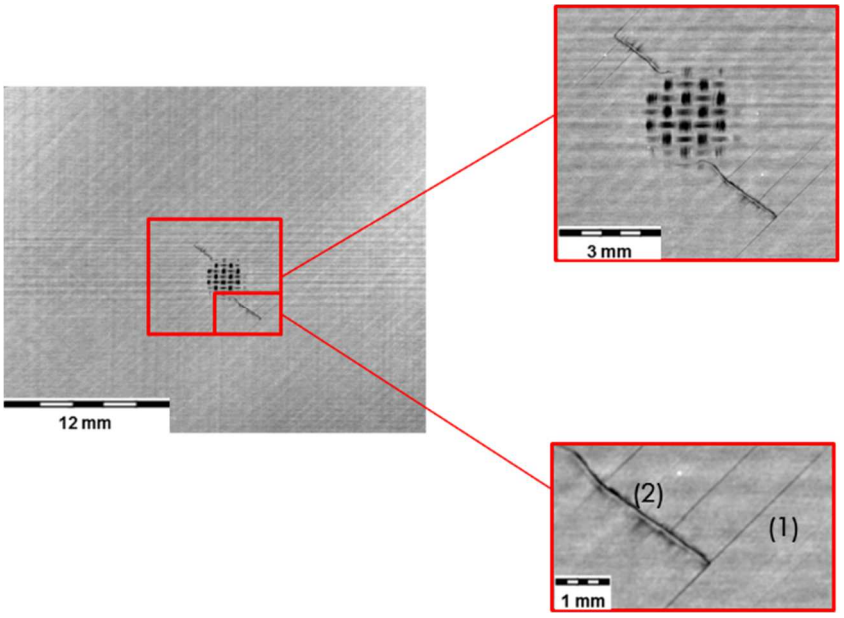

Fig. 12. µCT picture of an impact damage in a depth of 0.033 mm after an impact of 9.28 J. Top right: Detail view of the specimen on the left hand side. Intralaminar cracks transverse to the fiber direction and fiber cracks. Compressed area in the center. Bottom right: Details of intralaminar cracks transvers to fiber direction (1) and fiber cracks (2)

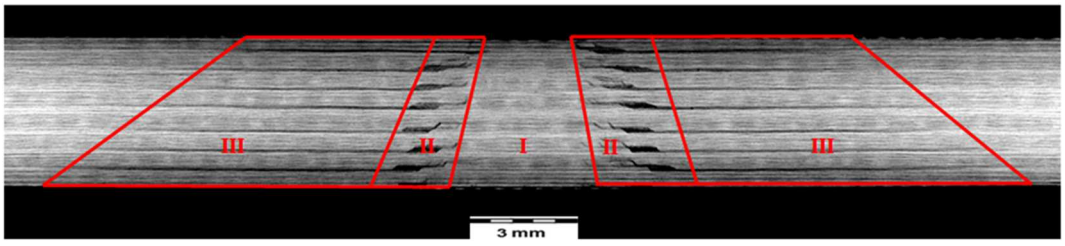

Fig. 13. µCT picture of the delaminated cross section. Segments of the damage morphology are: (I) compressed cone segment, (II) inner cone segment ring with intralaminar cracks, (III) outer cone segment ring with interlaminar cracks, i. e. delaminations. The complete impact damage morphology – consisiting of the above mentioned parts – is called delamination volume V_{del}

Fig. 12 bottom right provides a detailed view of the initial cracks on the impact side of the specimen. Damage (1) is an intralaminar crack within the first layer parallel to the fibers. These cracks between parallel orientated fibers indicate the orientation of the top layer as a +45° layer. Damage number (2) can be identified as a line of fiber cracks. This fiber failure line is perpendicular to the fiber direction. Different types of damage structures are shown in Figure 13. The delaminated cross section reveals three different cone segments.

Underneath the impactor there is the compressed inner cone segment (I). Due to the three-dimensional stress state with compressive loading perpendicular to the plies, no significant damage can be found in this area. The cone ring segment (II) contains the crack initiations. Here fiber cracks and intralaminar matrix failures can be found which lead the initial cracks to interlaminar delaminations.

Remarkable are the equal distances between the single horizontal delaminations in the outer cone ring segment due to the stacking sequence and the above mentioned mechanism of crack growth.

The additionally investigated impact parameters are shown in Figure 14.

The angle of the cone segment, the height of the cone, the cone base radius and the lateral extensions of delaminations are measured and compared to the other impact parameters.

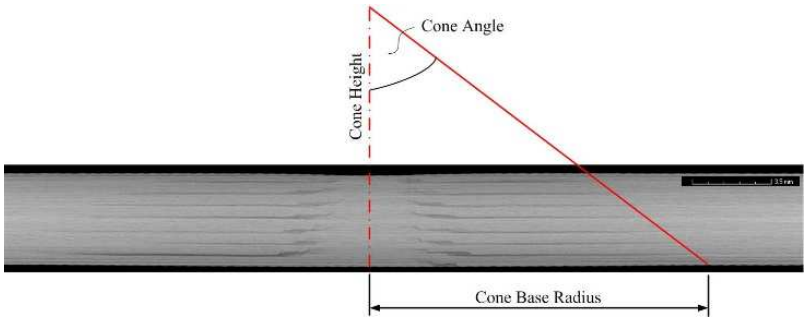

Fig. 14. Explanation of investigated damage parameters

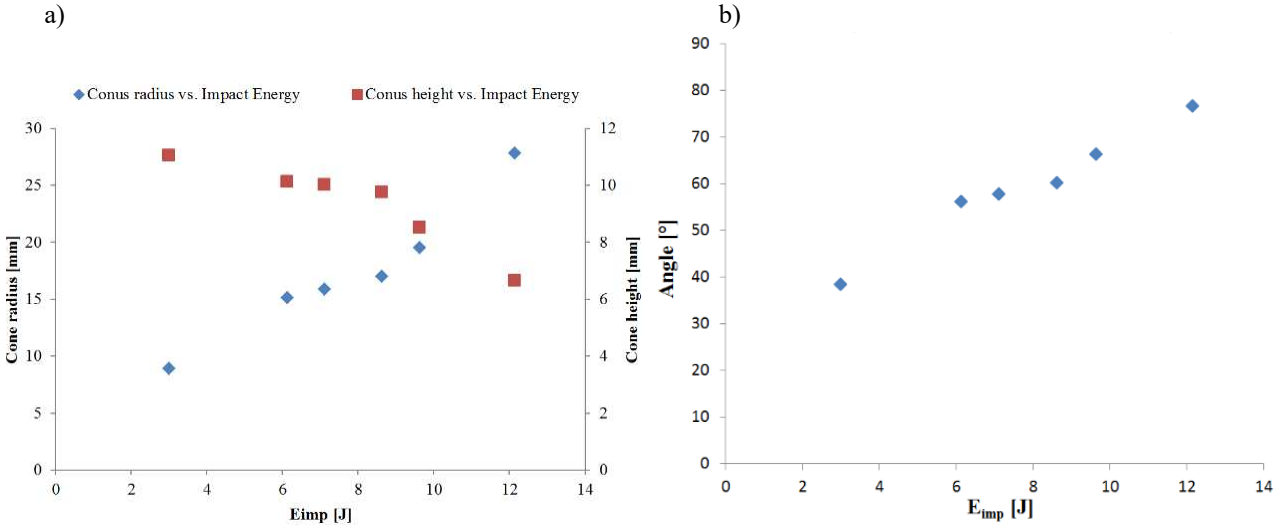

Fig. 15. a) Cone base radius and cone hight versus impact energy, b) Cone angle versus impact energy

Figure 15 displays the cone base radius and the cone height versus the impact energy. A quasi-linear correlation of the parameters can be seen. The correlations of cone radius versus impact energy and of cone height versus impact energy are shown with in Figure 16.

From figure 15 can be concluded, that the damage cone height flattens and the damage cone diameter increases with the amount of the impact energy.

The delamination volume increases with the dissipative energy. This correlation can be seen in Figure 16 a.

The relative delamination volume, i.e. the volume of the cone segments, in comparison to the dissipated energy versus all analyzed specimens, remains constant. This context is shown in Figure 16 b.

Crack initiation and crack growth is caused by the dissipated part of the impact energy. The necessary amount of energy for crack initiation and crack growth per square unit remains constant. Therefore, increasing impact energy together with an increasing cone base radius and a decreasing cone height result in an increasing delamination volume.

4. Conclusions

Impact delaminations in carbon fiber reinforced plastic are generated in a defined manner and with state of the art test equipment. A comparison is made between the results of well-established techniques such as Ultrasonic Testing or micrographic cross-sections with the results of Microfocus Computed X-Ray Tomography. The findings show that both Ultrasonic Testing and µCT show a linear correlation between impact energy and delaminated area. However, µCT is able to detect significantly larger delaminated areas. Other findings were that the undamaged zone immediately

underneath the contact point of the impactor is not a cylinder but a cone segment. The correlation between main impact parameters could be shown on the base of state of the art non-destructive testing.

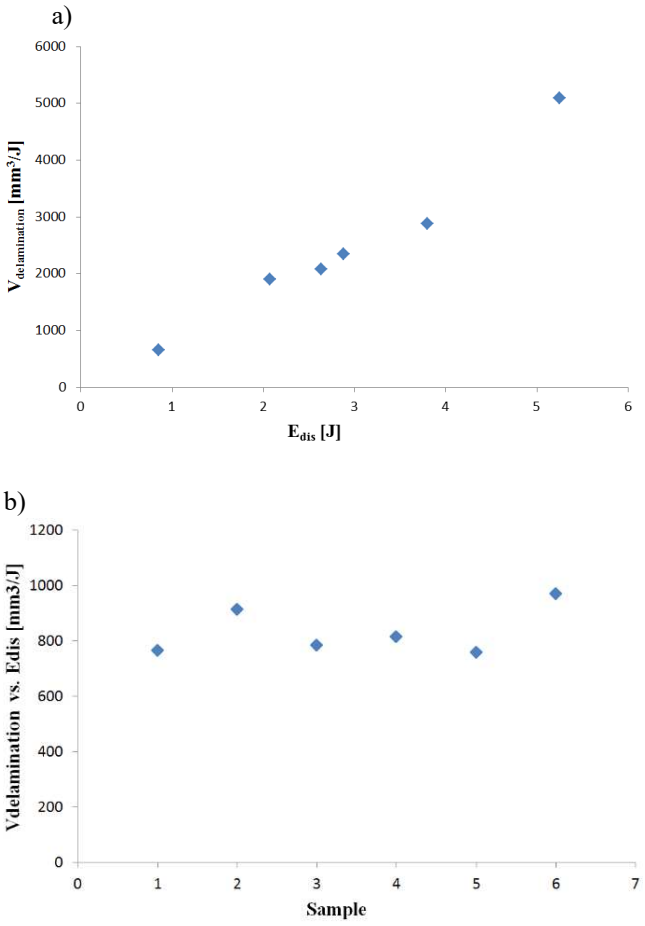

Fig. 16. a) Delamination volume versus dissipative energy, b) Cone segment volumina relativ to dissipative energies of the specimens

References

[1] N. N.http://www.hexcel.com/Resources/DataSheets/Prepreg-Data-Sheets/8552 eu.pdf, 12.07.2013

[2] N. N.: DIN EN 7000-11: Aerospace - Non-metallic materials - Rules for drafting and presentation of Werkstofformen - Part 11: prepregs. German standard,

[3] norm point Aviation (NL) at DIN Institute for Standardization e. V., Beuth Verlag GmbH, Berlin, 2000

[4] N. N.: DIN EN 2564: Carbon fiber laminates. Determination of the fiber, resin and amount of pores. German standard, norm point Aviation (NL) at DIN Institute for Standardization e. V., Beuth Verlag GmbH, Berlin, 1998

[5] N. N.: AITM 1.00.10: Fiber Reinforced Plastics. Determination of compression strength after impact. AIRBUS Industry Test Method, Lagnac Cedex, France, 1994.

[6] W.J. Cantwell, J. Morton, The impact resistance of composites materials – a review. Composites 22/5 (1993).

[7] W. Hilger, HFUS 2000 – Benutzerhandbuch. Ingenieurbüro Dr. Hilger, Braunschweig, 2000.

[8] H. Sekine, N. Hu, H. Fukanaga, T. Natsume, Low-velocity impact response of composite laminates with a delamination. Mechanics of Composite Materials and Structures, 1998, 275-278

[9] G. Zhou, L.J. Greaves, Damage resistance and tolerance of thick laminated woven roving GFRP plates subjected to low-velocity impact. Impact Behaviour of Fibre-Reinforced Composite Materials and Structures. CRC Press, Boca Raton (USA), 2000

[10] T. M.Tan,; C.T. Sun, Use of statical indentation laws in the impact analysis of laminacted composite plates. Journal of Applied Mechanics, Transactions of the ASME 52/6 (1985.)

[11] H.Y. ChoI,; C H. Lim, Low-velocity impact analysis of composite laminates using linearized contact law. Composite Structures 66 (2004) 125-132